PHYSICAL REVIEW B VOLUME 47, NUMBER 13 1 APRIL 1993-I

# Dislocation nucleation and crack stability: Lattice Green's-function treatment of cracks in a model hexagonal lattice

S. J. Zhou and A. E. Carlsson
*Department of Physics, Washington University, St. Louis, Missouri 63130*

Robb Thomson
*Materials Science and Engineering Laboratory, National Institute of Standards and Technology, Gaithersburg, Maryland 20899*

(Received 17 September 1992; revised manuscript received 20 November 1992)

A series of atomistic calculations is performed in order to evaluate the effects of several physical factors on dislocation emission in a model hexagonal lattice. The method of calculation is the lattice Green's-function method, together with several pair potentials with variable parameters. The physical factors of interest are the dislocation width (or, more precisely, maximum strain) and "unstable stacking energy" suggested by several continuum-based calculations, as well as the mode-I loading. We find that the continuum theories are surprisingly accurate, provided that some modifications are made. Typical discrepancies are of order 10% in the emission stress intensity. However, the atomistic calculations indicate that several of the assumptions underlying the continuum theories are inaccurate. In addition, we find strong mode-I–mode-II interactions, which are summarized in the form of a crack-stability diagram.

## I. INTRODUCTION

It is generally believed that a major factor in determining the ductile vs brittle behavior of materials is the ease of emission of dislocations from a crack tip. If dislocation emission is sufficiently easy, then a crack will respond to an applied stress by such emission, and concomitant plastic deformation, rather than by crack extension. Nearly two decades ago, Rice and Thomson[1] developed a semiquantitative criterion for ductile vs brittle behavior based on a balance of forces on the dislocation due to the applied stress and the image force. For the "mode-II emission configuration" where the dislocation is emitted on the cleavage plane ahead of the crack, continuum elasticity theory predicts that the critical value of the stress intensity for dislocation emission, $K_{\mathrm{IIe}}$, is[2]

$$K_{\mathrm{IIe}} = \mu b/(1-\nu)\sqrt{8\pi r_c}, \tag{1.1}$$

where $\mu$ is the shear modulus, $b$ is the Burgers vector of the emitted dislocation, and $r_c$ is an empirical core cutoff parameter. For physically reasonable values of $r_c$, the ductile-to-brittle transition then occurs at approximately $\mu b/10\gamma_s = 1$, where $\gamma_s$ is the surface energy. If $b$ is large, then the creation of the dislocation requires a large energy barrier, which tends to cause brittleness; if $\gamma_s$ is large, then ductility is enhanced because crack propagation is made more difficult. This criterion successfully correlates a large body of experimental data. However, there is not a precise prescription for obtaining the dislocation core cutoff parameter $r_c$.

This analysis has been extended by several workers, including Weertman,[3] Schoeck,[4] and Rice.[5] Of particular interest here are the treatments of Rice and Schoeck. Both of them have reanalyzed the Rice-Thomson criterion on the basis of the Peierls approach (see Hirth and Lothe[6]), in which the emitted dislocation is viewed within continuum theory as a continuous distribution of infinitesimal dislocations. Rice assumed a periodic relation between shear stress and a continuously defined sliding displacement $\delta(r)$ along a crystal slip plane emanating from a crack tip. Three energy terms were then included: the energy of the sliding displacement, the interaction energy of the (partly formed) dislocation with the external stress field, and an elastic self-energy term from the dislocation, whose form reflects the presence of the crack. Finally, it was demonstrated that emission would occur precisely when the dislocation is half-formed, i.e., $\delta(r) = b/2$ at the crack tip. For the simplified case of pure mode-II loading and coincident crack and slip planes, it was possible to obtain an exact solution to the force-balance equations for $\delta(r)$, and thus an emission criterion. Rice identified a solid-state parameter, the unstable stacking energy $\gamma_{\mathrm{us}}$, which characterizes the resistance to displacement along the slip plane, and thus to dislocation nucleation. It is the maximum energy barrier encountered in blocklike sliding along the slip plane, of one-half of the crystal relative to the other. Thus it provides the simplest measure of the effects of the discreteness of the crystal structure. In terms of $\gamma_{\mathrm{us}}$, the emission criterion is as follows:

$$K_{\mathrm{IIe}} = \sqrt{2\gamma_{\mathrm{us}}\mu/(1-\nu)}. \tag{1.2}$$

This approach has the advantage that there is no need to introduce an empirical cutoff parameter; in fact, $\gamma_{\mathrm{us}}$ can be accurately calculated by several existing first-principles total-energy methods. However, the theory contains approximations which need to be tested, for

example the assumption that the inhomogenous distribution of displacements around a dislocation can be described by the homogeneous displacements entering $\gamma_{us}$.

Schoeck[4] uses a distribution of infinitesimal dislocations as well, in a continuum theory based on an approximation of the Peierls analysis, with an explicit image force term. Rather than exactly solving the force-balance equations, Schoeck simplifies the problem by assuming a fixed analytic form for the distribution of infinitesimal dislocations:

$$\beta(x) = (b/\pi)w/(x^2 + w^2),$$

so that the displacement $\delta(x)$, the (negative) integral of $\beta(x)$, is given by

$$\delta(x) = b/2 - (b/\pi)\arctan(x/w), \tag{1.3}$$

where the integration constant is chosen so $\delta$ goes to zero far from the crack tip. Here $x$ is measured relative to the center of the dislocation. The critical parameter in the theory is then the dislocation half-width $w$. We will find it convenient to replace $w$ by the maximal strain $\eta$ in the dislocation distribution, because this quantity can be readily evaluated in our simulations. Clearly, the two parameters are equivalent, as, according to Eq. (1.3), $\eta = b/\pi w$. These parameters are the simplest description of the structure of the emerging dislocation. They are related (although certainly not equivalent) to $\gamma_{us}$; as we shall see in Sec. III B, a small value of $\gamma_{us}$ leads (within the Peierls approach) to a large value of $w$ and thus a small value of $\eta$. Thus, a small value of $\eta$ corresponds to easy dislocation emission.

By evaluating the energy of the emerging dislocation distribution as a function of position, Schoeck was able to calculate the value of $K_{II}$ at which there was no energy barrier to emission; this value was taken to be $K_{IIe}$. The numerically obtained result is

$$K_{IIe} = [0.69\mu/(1-\nu)]\sqrt{\eta b}. \tag{1.4}$$

The similarity of this criterion to the Rice-Thomson criterion Eq. (1.1) suggests that $1/\eta$ may be thought of as a more precisely defined version of the Rice-Thomson parameter $r_c$. Again, there are several approximations that need to be tested, in particular the assumption that the shape of the dislocation is unaffected by the presence of the crack. In addition, the empirical parameter $\eta$ is not obtained from the theory, but must be obtained from atomistic simulations.

In this paper, we aim to obtain a more precise description of the criterion for dislocation emission, via atomic simulations. We use our lattice Green's function method (Thomson *et al.*[7]) in the mode-II emission configuration to study the fracture behavior of a two-dimensional hexagonal lattice. Although the mode-II emission geometry is, of course, idealized, it allows us to see in the simplest possible fashion some of the effects which must also be present in more complex systems. In particular, mode-I and mode-II loadings act independently within elasticity theory, but in our atomistic model it is possible to identify directly the interactions between the different loadings. We obtain numerical estimates of the critical stress $K_{IIe}$ required for dislocation emission for several pair-potential-type force laws, and find that the dislocation maximum strain $\eta$ describes our results very accurately. We then compare our results to those of Schoeck and Rice, and finally develop a crack-stability diagram which illustrates the interactions between mode-I and mode-II loading.

Although this paper focuses on the simplified case of dislocation emission along the crack plane, the methodology is entirely applicable to the more physically interesting case in which the dislocation emerges on another slip plane. This case will be treated in a subsequent publication.

## II. DESCRIPTION OF CALCULATION

### A. Crystal geometry and elastic parameters

Our two-dimensional (2D) hexagonal model lattice with a crack is depicted in Fig. 1. In our calculations, the supercell size is $4 \times 10^6$, and the total allowed crack length, $2l_{max} + 1$, is 101 lattice spacings; the allowed length of the cohesive zone at the crack tip where the bonds are "nonlinear" (neither completely broken nor linear) is 20. (See Thomson *et al.*[7]) for further discussion of these parameters.) The actual crack length $l_c$ is then determined by the number of broken bonds. Note that the cohesive zone is placed at only the right-hand side of the crack; at the left-hand side, all of the bonds up to the end of the allowed crack region are assumed broken. The external load, $F$, for the system is a pair of oppositely directed forces applied to the two atoms (top and bottom) at the center of the allowed crack region. The force $F$ contains both tensile and shear components. For each value of $F$, we achieve mechanical equilibrium, with a convergence criterion corresponding to all atoms moving less than $10^{-3}$ lattice spacings in a self-consistency iteration.

In comparing the 2D calculations with the conventional plane strain elastic equations quoted in Eqs. (1.1)–(1.4) above, there is a fundamental point which must be kept in mind. The 2D model is not 3D plane strain. However, it is equivalent to 3D plane stress. To see why, consider

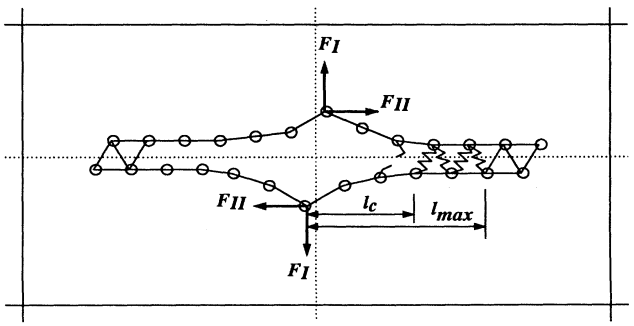


FIG. 1. Schematic of crack geometry and application of forces.

a 3D lattice composed of layers of our 2D lattice stacked above one another in the third dimension. If the 3D lattice is then given a plane strain (displacements in the direction normal to the 2D layers are zero), the atoms lying in layers above and below a reference layer will exert forces on the atoms of the reference layer, because of the strained bonds between the layers. This is a Poisson's ratio effect. In our problem, these forces are not allowed. In 3D plane stress, a displacement between the layers occurs such that no forces are transmitted from one layer to another. This means that so far as the in-plane stress and strains are concerned, the additional layers do not contribute, and the plane stress 3D problem yields the same result within the plane as the actual 2D problem we simulate. Thus, we must compare our 2D simulations with plane stress predictions, not the plane strain predictions in Eqs. (1.1)–( 1.4). The conversion of plane strain results to plane stress equations is very simple: One must convert every factor $(1-\nu)$ in Eqs. (1.1)–(1.4) into the factor $1/(1+\nu)$. In our lattice, $\mu = k\sqrt{3}/4$ and $\nu = 1/4$, where $k$ is the spring constant. Thus there is a correction factor of 6% and 3% between the plane strain and plane stress emission predictions of Schoeck and Rice, respectively, which we will fold into the comparisons we make below. The reader may note that we have quoted the value for $\nu$ appropriate for a 3D medium, not that for 2D. This is necessary in order to be consistent with using the 3D continuum equations in plane stress.

Our results will be given in terms of stress-intensity factors, which from elasticity theory for a finite crack (see Thomson[2]) are given by

$$K_{\mathrm{I,II}} = \frac{F_{\mathrm{I,II}}}{\sqrt{\pi c}}\sqrt{\frac{c+t}{c-t}}. \tag{2.1}$$

(The reader will note that the expressions for stress-intensity factors are the same in both plane strain and plane stress.) In this equation, we have introduced the usual continuum parameters, $c$, equal to half the length of the broken-bond region (cf. Fig. 1), and $t$, the lattice position where the force is applied, relative to the crack tip. In our case, the length of crack is complicated because the crack "tip" will lie at some point within the cohesive zone, and the particular atomic solution will determine where this is. We choose the atomic crack tip to be the point were the forces exerted across the cleavage plane are the greatest, and the center of the dislocation to be the atom pair where the relative displacement across the cleavage plane is closest to a half lattice spacing; for the triangular lattice this corresponds to the atoms being precisely above and below one another. Thus, with the loading prescription used here, $K$ will decrease as the crack propagates under fixed load. By comparing the Griffith value for the critical stress intensity (in plane stress) required to propagate the crack,

$$K_{\mathrm{Ic}} = 2\sqrt{\gamma_s \mu(1+\nu)}, \tag{2.2}$$

with the numerical results from our simulations, we find that the continuum relation (5) is accurate to within a few percent for our atomistic calculations, provided that $l_c$ exceeds 30 lattice spacings. In our lattice, $\mu = k\sqrt{3}/4$ and $\nu = 1/4$, where $k$ is the spring constant.

### B. Force laws

In this work, we use a variety of pair-potential-based force laws. In all of these, we choose the parameters so that the elastic spring constant $k$ is the same, in order to facilitate comparisons; nevertheless, the surface and unstable-stacking energies can be varied considerably. In addition, we cut the force off at the second-neighbor distance $\sqrt{3}a$, where $a$ is the lattice constant. A constant is then added to the pair-potential functions given below, in order to make them continuous at the cutoff distance. The truncation effects are the largest for the "Cu" parameters ($F^{\mathrm{UBER}}$ below with $l = 0.19$); here small cutoff-induced trapping effects are observed. In the other cases, the truncation effects are negligible. The force laws are illustrated in Fig. 2. The first is the universal binding energy relation (UBER) of Rose, Smith, and Ferrante.[8] Here, the pair force is given by

$$F^{\mathrm{UBER}} = -k(r-a)e^{-(r-a)/l}, \tag{2.3a}$$

which is derived from the pair potential

$$V_2 = -kl^2[1+(r-a)/l]e^{-(r-a)/l}, \tag{2.3b}$$

where $k$ is the linear spring constant, $r$ is the interatomic separation, and $l$ is the force law decay-length parameter. We will always express $l$ in units of $a$. Several values of $l$ are used to elucidate the chemical trends as clearly as possible; although not all of these necessarily correspond to real materials, the variation of $l$ is a useful stratagem in exploring brittle vs ductile behavior.

In order to obtain a wider range of force laws, we have modified the attractive part ($r > a$) of the force laws in several ways (but always keeping the UBER repulsive part). In all these additional cases, we have retained the "Cu" values for $k$ and have chosen $l$ so that the bond

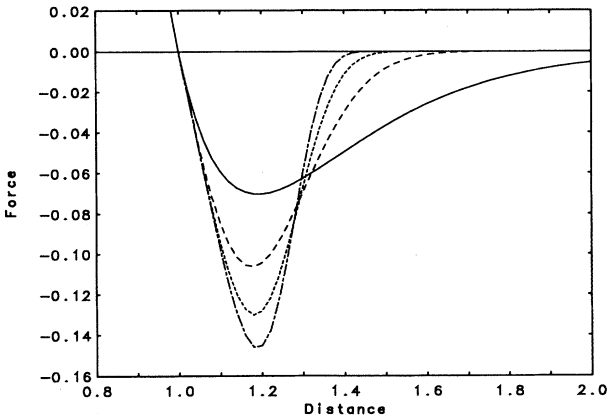


FIG. 2. Force laws used in atomistic simulations. Solid curve, $F^{\mathrm{UBER}}$ with $l = 0.191$; long-dash curve, $F^a$ with $l = 0.248$; short-dash line, $F^b$ with $l = 0.262$; long-short dashes, $F^c$ with $l = 0.266$. Distance in units of $a$, force in units of $ka$.

strength is also the same as for "Cu," unless stated otherwise.

$$F^a = -k(r-a)e^{-(r-a)^2/l^2}, \tag{2.3c}$$

$$F^b = -k(r-a)e^{-(r-a)^3/l^3}, \tag{2.3d}$$

$$F^c = -k(r-a)e^{-(r-a)^4/l^4}. \tag{2.3e}$$

Of these, $F^a$ corresponds to a pair potential with Gaussian form; in the remaining cases the pair potentials were obtained by numerical integration of the force.

### C. Evaluation of $K_{IIe}$

Our results for $K_{IIe}$ are obtained for both equilibrium and nonequilibrium cracks. By an equilibrium crack, we mean one which is in stable static equilibrium consistent with the force laws at its tip. A nonequilibrium crack is one where we have arbitrarily cut the bonds, and not allowed the bonding forces to reconnect themselves across the cleavage plane, even when the atoms are within range. This is a mathematical trick used ubiquitously in fracture mechanics. Thus, a pure mode-II nonequilibrium crack is one where no mode-I loadings are exerted to open the crack tip, but a mathematical knife is invoked to cut the bonds across the cleavage plane behind the crack tip (i.e., to the left of the crack tip in Fig. 1). This is the atomic analogue of Rice's mode-II construction. We have also constructed other nonequilibrium solutions, where the mode-I load is greater than zero, but is not sufficient to hold the atoms apart, in equilibrium, against their bonding forces at the tip.

Although in this way, we are able to construct an atomic analogue of the continuum mode-II crack, there is an important distinction to be made between the atomic and continuum cases. In the continuum, there is no vertical displacement on the cleavage plane ahead of the mode-II crack. In the atomic case, there is, because of the response of the hexagonal lattice to the horizontal mode-II shear force. This causes a closure of the crack tip, with an effective compressive mode-I loading there. It is an unavoidable result of the lattice, not to be confused with the "Poisson ratio effect," and leads to results which have no analogue in the continuum mode-II case. In comparing our mode-II results with those of Rice, this distinction must always be kept in mind.

Typical crack atomic configurations are shown in Fig. 3, which displays the atoms in the cohesive zone at the end of the crack (where nonlinear bonds are attached). In all three frames, the crack tip is well defined in terms of the maximum force exerted across the cleavage plane. The various values of $K_{I,II}$ are determined from Eq. (2.1), with the measured position of the crack tip, and the input loads. In Fig. 3(a), the crack is loaded by a purely tensile force. In Fig. 3(b), the tensile force is the same as in Fig. 3(a), but a shear component is added. An incipient dislocation (before emission) is seen, whose position is indicated in the figure. Figure 3(c) shows the configuration after the shear component is increased slightly. The dislocation has now been emitted. It stops at the end of the cohesive zone, because from this point on, the bonds are linear and therefore cannot break. In effect, the end of the cohesive zone acts as a strong pinning point. $K_{IIe}$ is obtained from our calculations as the value of $K_{II}$ corresponding to Fig. 3(b), i.e., just before emission.

In order to see the dislocation properties in a more quantitative manner, we examine the horizontal relative displacement, $\Delta u(x)$, across the cleavage plane. That is, we compare the displacement on the upper cleavage plane, $u^+(x_i)$ with that of the corresponding atom on the lower cleavage plane, $u^-(x_i)$. $\Delta u(x_i) = u^+(x_i) - u^-(x_i)$. Figure 4(a) shows the results for the equilibrium case, with varying mode-II loading. We see that a dislocation is built up gradually with increasing mode-II loading. The center of the dislocation (emerging or fully formed) is at the point of maximum slope in the curve, which defines the parameter, $\eta$. Once the dislocation is emitted (upper curves), a well-defined region of fairly "perfect" crystal is seen between the dislocation and the crack tip. Figure 4(a) also shows that the position of the crack tip wanders somewhat during the emission process. The amount of this wander depends upon the force law, and is a general characteristic of the emission process. Figure 4(b) again shows the equilibrium case, but with focus on two values of $K_{II}$, immediately before and after emission. For subsequent use, a comparison with the form of Schoeck [Eq. (1.4)] is shown.

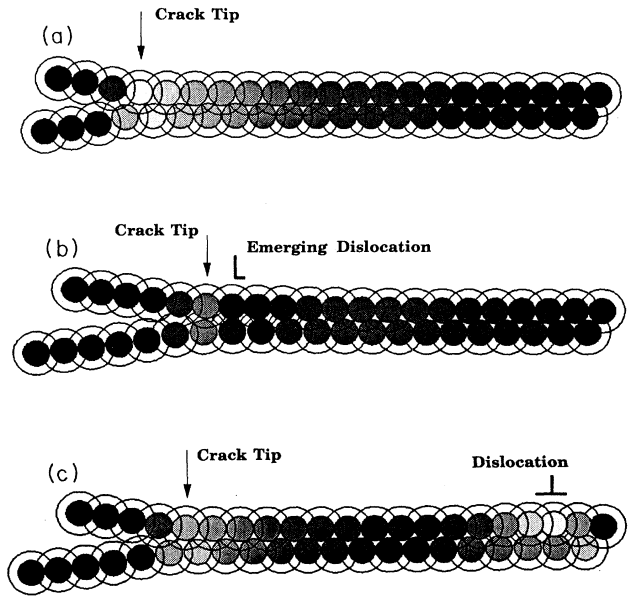


FIG. 3. Crack geometries. (a) Pure mode-I crack. Arrow denotes crack-tip position. (b) Equilibrium crack just before emission. The "half dislocation" symbol denotes the center of the emerging dislocation. (c) Equilibrium crack after emission. The filled circles denote atom size in the equilibrium lattice, the outer circle about each atom center gives the range of the force law, and the density of filling denotes the magnitude of the total force on an atom transmitted to it across the cleavage plane. Full black denotes zero force, full white maximum force.

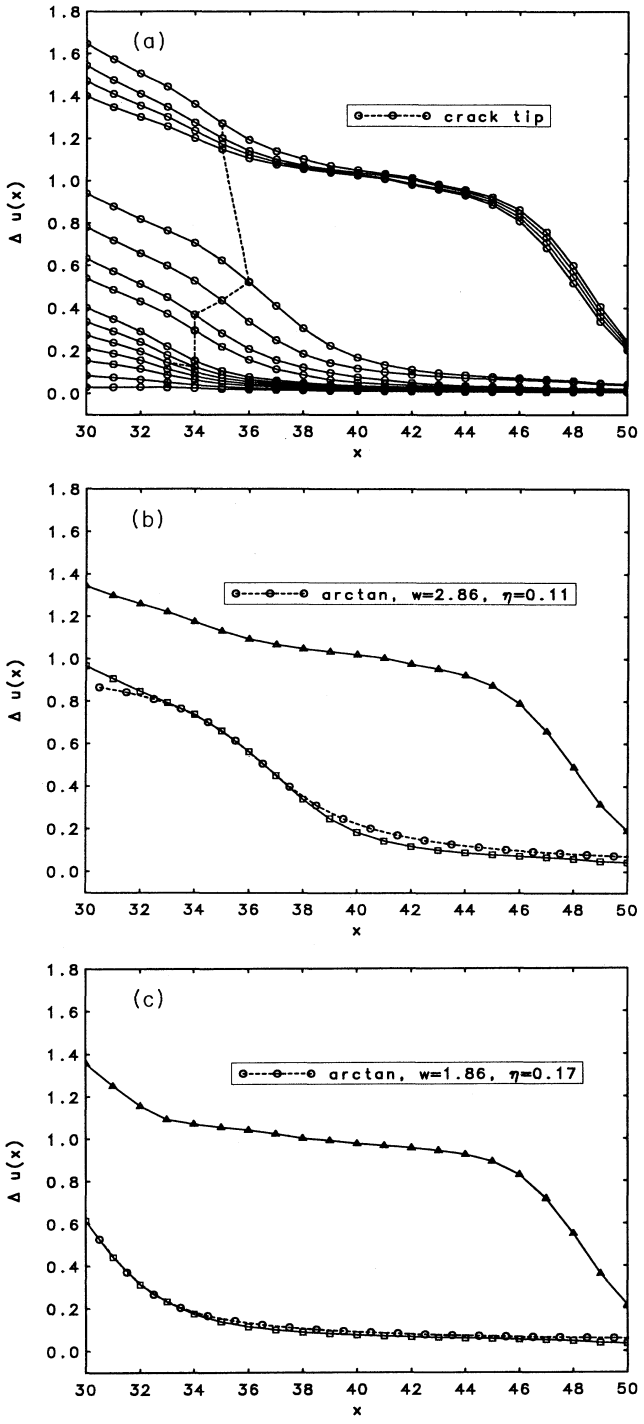


FIG. 4. Horizontal relative displacements, $\Delta u(x)$, vs horizontal position $x$. (a) and (b) Equilibrium crack. (c) Pure mode-II nonequilibrium crack. Displacements and positions are given in units of $a$. Frames (b) and (c) include fit to Eq. (3) for dislocation shape (connected circles). In frame (a) $K_{\rm I}$ is fixed at 0.261, while $K_{\rm II}$ ranges from 0.005 to 0.015; emission occurs at approximately $K_{\rm II} = 0.11$. In frame (b), curves are for $K_{\rm II} = 0.109$ and 0.110; in frame (c), curves are for $K_{\rm II} = 0.136$ and 0.137. The best values of the dislocation width, $w$ and maximum strain, $\eta$, to fit the arctan function are listed on the figures in (b) and (c).

Figure 4(c), shows the horizontal displacements for the nonequilibrium mode-II case. Again, the dislocation is well separated from the crack tip after emission.

We list values of stress intensity in Fig. 4 as calculated from the computed structure and Eq. (2.1). However, the variation of $K$ in Fig. 4(b) for the two structures, for example, just before and just after emission is only about 1%. When the crack tip structure changes drastically, as it does between these two cases, the value of $K$ cannot be inferred to such accuracy. The reader should simply know that the actual force exerted at the center of the crack does increase in the way implied from the reported values of $K$.

## III. RESULTS

### A. Effects of force law on $\gamma_s$, $\gamma_{\rm us}$, and $\eta$

Before turning to our numerical results for $K_{\rm IIe}$, we discuss in general terms the effects of the atomic force law on the basic parameters that we expect to be relevant for fracture. In the Rice-Thomson model, brittle vs ductile behavior is defined by whether or not the conditions for dislocation emission for a crack in mode-I configuration are met prior to Griffith cleavage. Although the present work treats cracks in mode-II configuration, the behavior of the emission criterion vs the cleavage condition is still relevant to the more general brittle or ductile issue in the mode-I configuration. The mode-I configuration will be addressed in a separate paper.

The chemical trends associated with changing the force law are most easily studied in the context of the UBER with fixed spring constant, $k$. Thus, as mentioned above, we will generally keep $k$ fixed at the "Cu" value. Under that assumption, there is only one parameter which affects the competition between cleavage and emission—the (dimensionless) length-scale parameter $l$. Results for the surface energy $\gamma_s$, the unstable stacking energy $\gamma_{\rm us}$, the critical mode-II energy release, $\mathcal{G}_{\rm IIe} = K_{\rm IIe}^2/2\mu(1+\nu)$, and the dislocation maximum strain, $\eta$, are given in Fig. 5 as functions of $l$. [This expression for $\mathcal{G}_{\rm IIe}$ is written for plane stress. Compare Eq. (1.2).] We evaluate $\gamma_{\rm us}$ using the condition that the vertical component of the force between the two sliding blocks vanish, as suggested by Rice.[5] In our simple model, $\gamma_s$ is equal to the value of the pair potential at the nearest-neighbor separation, because each surface atom loses two neighbors by the creation of the surface. In the UBER formulation, we see by Eq. (2.3b) that this is roughly proportional to $l^2$, as is seen in Fig. 5. On the other hand, $\gamma_{\rm us}$ first increases with increasing $l$, then reaches a maximum, and finally decreases. For small $l$, the increase in $\gamma_{\rm us}$ is due to the increase in depth of the potential discussed above; for a vanishingly deep potential, $\gamma_{\rm us}$ must of course vanish. As $l$ increases further, the potential becomes broader, and the corrugations in the energy as a function of displacement are reduced. This results in $\gamma_{\rm us}$ possessing a maximum as a function of $l$. Note that over the whole physically relevant range of $l$, $\gamma_{\rm us}$ varies less than $\gamma_s$. The reader will note that the small vari-

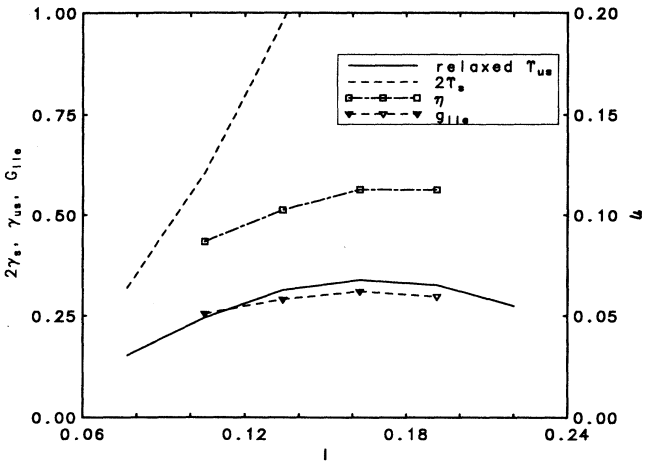


FIG. 5. Dependence of twice the surface energy $2\gamma_s$ (dashed line), unstable stacking energy $\gamma_{us}$ (solid line), $\mathcal{G}_{IIe}$, (connected triangles), and dislocation maximum slope $\eta$ (connected squares) on length-scale parameter $l$ in UBER force law. $\eta$ is dimensionless, and is plotted on the right axis, the other three quantities are plotted on the left in units of $2\gamma_{us}$(Cu). $\mathcal{G}_{IIe}$ is plotted for the plane stress predictions discussed in the text.

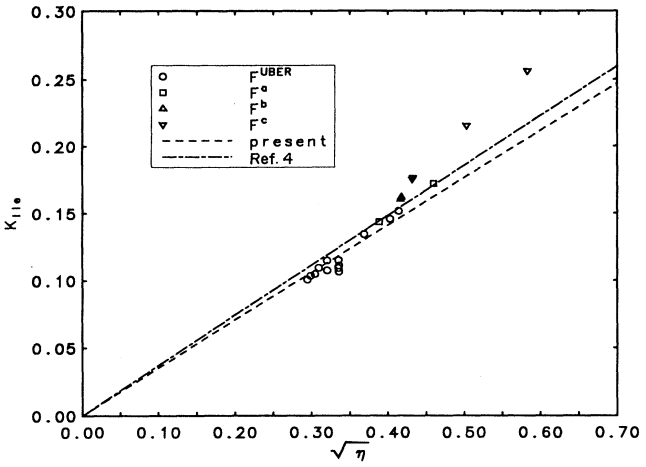


FIG. 6. Atomistic results for $K_{IIe}$ vs square root of dislocation maximum strain. Dashed line denotes linear fit to UBER points; dot-dashed line is result of Schoeck. Points for various force laws labeled in box. Units of $K$ are $(k\sqrt{a})$. The Schoeck results, Eq. (1.4), have been altered for plane stress conditions.

ations in $\eta$ observed with varying $l$ are similar to those in $\gamma_{us}$. We have plotted the parameter $\mathcal{G}_{IIe}$ in order to track Rice's criterion, Eq. (1.2), with the parameter $l$.

At this point, we are in a position to compare the relative magnitudes of $K_{Ic}/K_{IIe}$, which is the analogue in the present case of the intrinsic ductility criterion introduced by Rice and Thomson, and discussed briefly in the Introduction. Because $K_{Ic}$ is controlled by $\gamma_s$, and $K_{IIe}$ is probably closely related to $\gamma_{us}$ and $\eta$, we believe that the increase of $\gamma_s$ relative to $\gamma_{us}$ and $\eta$, shown in Fig. 5, can lead to a crack switching from brittle to ductile behavior with increasing $l$. The fact that the curve for $2\gamma_s$ is always above $\gamma_{us}$ means that at least for reasonable values of $l$, the UBER force law is always "ductile" in this sense for the mode-II configuration.

### B. Maximum-slope criterion

Results for $K_{IIe}$ for the various force-law types and parameters that we have used are given in Fig. 6. Here, we show results for both equilibrium and nonequilibrium cracks. The horizontal axis is $\sqrt{\eta}$, as is suggested by Schoeck's analysis [cf. Eq. (1.4)]. We find that $K_{IIe}$ is determined very accurately by $\eta$, as evidenced by the figure. Our results combine both fully equilibrium and nonequilibrium cases where the mode-I load is not sufficient to open the crack, as well as pure mode-II cases. All cases can be plotted on the same trend line, so we have not distinguished equilibrium from nonequilibrium in the figure. Here, the dashed line is a fit to the UBER results, which we consider the most physical. We note that this correlation is predicted already by Eq. (1.1). We expect $r_c$ to be roughly inversely proportional to $\eta$. Thus $K_{IIe} \propto \sqrt{\eta}$, in agreement with the results of Fig. 6, and with Eq. (1.4).

### C. Evaluation of Schoeck's model

Schoeck's model provides an evaluation [cf. Eq. (1.4)] of the proportionality constant relating $K_{IIe}$ to $\sqrt{\eta}$. We see in Fig. 6 that his constant provides agreement with the atomistic results at roughly the 10% level. In order to test his assumptions, we have evaluated the quality of fit that is obtained by Eq. (1.3) for the dislocation shape. As indicated in Figs. 4(b) and 4(c), the quality of fit is quite good for the UBER force law. In the pure mode-II (nonequilibrium) crack, the center of the dislocation is right at the crack tip, while in the equilibrium case it is shifted by about one lattice constant. We find that although the arctan is a good fitting function for the UBER, it is less so for the force law, $F^c$ in Eq. (2.3e). $F^c$ is, of course, an extreme case, and not very "physical," but it gives us a sense of the limits of the theory. As Schoeck states, the assumptions in his development make one expect that his prediction for $K_{IIe}$ will be an upper limit. Figure 6 shows that expectation is valid for the UBER, but not for the other force laws.

We are also able to test Schoeck's assumption that the width of the dislocation is the same in the crack core as in the free lattice. The Peierls analysis (Rice[5]) finds a ratio of two between the two values, with the crack-tip dislocation being wider. Our results, for an equilibrium crack, are given in Fig. 7. We see that the ratio depends on the force law, but is in the range of 1.4 for UBER. The origin of the dislocation width change is a very important question in the interpretation of our results. This result can be understood via either of the two simplified models that are most used to describe dislocation structure, namely the Peierls model used by Schoeck and Rice, and the Frenkel-Kontorova model. If, in Rice's approach, one assumes that the misfit function $\Phi(\delta)$ has a sinusoidal form, with a maximum value of $\gamma_{us}$, then the usual Peierls analysis (Hirth and Lothe[6]) goes through

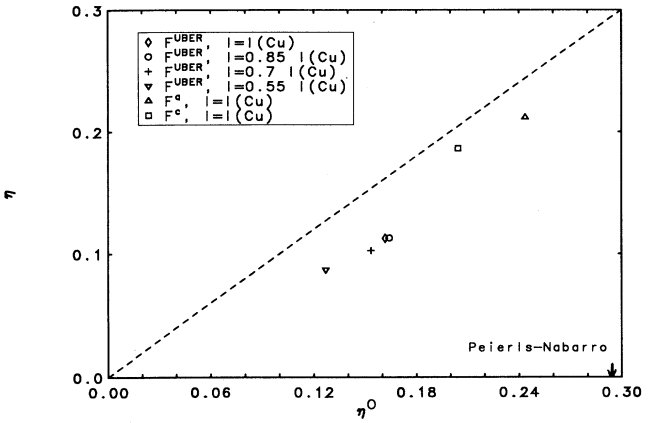


FIG. 7. Relation between bulk dislocation maximum strain $\eta^0$ and crack-tip dislocation maximum strain $\eta$. Dashed line is locus of equality between $\eta$ and $\eta^0$. The Peierls-Nabarro model in the free lattice is shown on the horizontal axis at $\eta^0 = 0.276$. Points for various force laws are noted in the figure box.

basically untouched, except that the force-balance equation is replaced by

$$\int_{-\infty}^{\infty} \beta(x')dx'/(x-x') = -[4\pi^2(1-\nu)\gamma_{us}/\mu b]\sin\{2\pi\delta(x)/b\}, \quad (3.1)$$

where $\beta(x) = -d\delta/dx$. Here $\delta$ is twice the displacement $u$ of Hirth and Lothe. The solution to this has the form of Eq. (1.3), but with a width $w = \mu b^2/8\pi^2(1-\nu)\gamma_{us}$. Thus the width is inversely proportional to $\gamma_{us}$. Foreman, Jaswon, and Wood[15] have studied numerical extensions of the original Peierls treatment for force laws other than the sinusoidal, and report that the core width is inversely proportional to the maximum stress. This is in qualitative agreement with the prediction from Eq. (3.1), because $\gamma_{us}$ is expected to be roughly proportional to the maximum stress. Alternatively to the Peierls analysis, in the Frenkel-Kontorova model (see Frank and Steeds[9]), the dislocation structure is determined by two parameters, the in-plane force constant $\alpha$, and the magnitude of the corrugations in the potential associated with atomic planes sliding over one another. The former quantity may be associated with $\mu$, and the latter with $\gamma_{us}$. The Frenkel-Kontorova analysis indicates that $w \propto \sqrt{\alpha}/\gamma_{us}$. Thus, the content of all these results is that large corrugations tend to narrow the dislocation core, while a large shear elastic constant tends to expand it.

One would expect that the tensile stress across the slip plane exerted by the mode-I component of the load on an equilibrium crack would increase the interplanar spacing, and thereby reduce $\gamma_{us}$; on the other hand, the shear constant remains constant (in the Frenkel-Kontorova model, it is only the in-plane shear constant that enters). Thus we have one tentative explanation of the change in the dislocation width at the crack tip, based on the tensile stress in that region. The importance of the tensile stress is confirmed by the result that for the pure mode-II crack (no applied tensile stress), the dislocation just before emission is actually 5% narrower than in the bulk. The reason for the decrease in width is that for pure mode-II stress in the hexagonal structure, the region around the crack tip is indirectly compressed by the hexagonal lattice response to shear loads as discussed at the start of this section. This compression is overcome by the tensile loading for an equilibrium crack. In addition to the tensile stress, the core of the emerging dislocation is also broadened by its image in the crack tip. Since the pure mode-II emerging dislocation is narrowed as noted above, clearly the major influence on the crack core is the tensile stress in that case.

Because Schoeck's approach is continuum based, it has no Peierls barrier to the motion of the dislocations. The Peierls barrier increases in going from $F^a$ to $F^b$ to $F^c$, and the plotted values of $\eta$ in Fig. 6 also increase monotonically, relative to Schoeck's curve, in the same sequence. Thus, the deviation of the points in Fig. 6 from Schoeck's prediction seems to be simply explained by the neglect of the Peierls barrier in his work.

In summary, we find that our results are well described by a relation of the form of Eq. (1.1), with

$$r_c \simeq b/10\eta. \quad (3.2)$$

Finally, Shoeck makes the important assumption that during the emission process, the crack tip is held rigidly in place. We find, in fact, that the crack wanders first forward and then backward as the dislocation emerges. This wandering of the crack during emission is an important feature of all our emission simulations, and comes up again in Sec. III F below.

### D. Evaluation of Rice's criterion

Comparison of the present atomistic results with Rice's continuum results is given in Fig. 8. We give results for

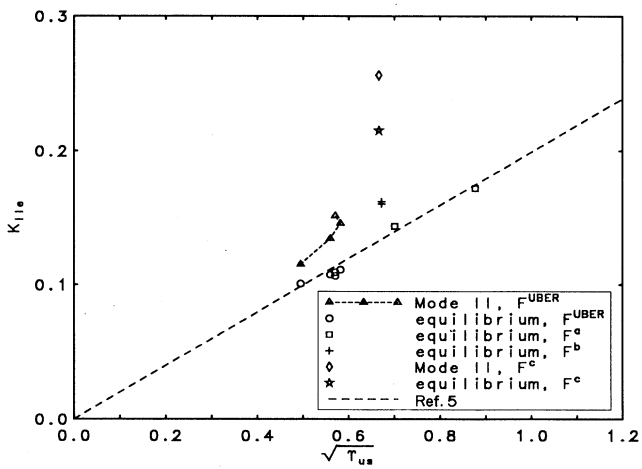


FIG. 8. Atomistic results for $K_{IIe}$ vs square root of unstable stacking energy $\gamma_{us}$. Dashed line denotes result of Rice, altered for plane stress conditions. Triangles are for pure mode II, while circles are for full equilibrium crack. Points for various force laws labeled in box. Units of $K$ are $(k\sqrt{a})$ and $\gamma_{us}$ are $\gamma_s$ (Cu).

pure mode II, as per Rice, as well as for the fully equilibrium crack. For pure mode-II loading, we find that $K_{IIe}$ exceeds Rice's values by 15–30 %, depending on the force-law parameters. This level of agreement is quite impressive, given the absence of adjustable parameters in the theory, and its quasicontinuum nature. In the equilibrium crack, the mode-I loading reduces $K_{IIe}$ for reasons to be discussed in Sec. III F. Here, surprisingly, $K_{IIe}$ is closer to Rice's values than for the pure mode-II case. Thus Rice's model actually gives more accurate results for the equilibrium crack. In this case, the discrepancies are approximately equivalent to those of the Schoeck theory. The trends with changing $l$ are also obtained more accurately in the equilibrium crack, in that $K_{IIe}$ increases weakly with increasing $l$ (cf. Fig. 5) in both the atomistic results and in Rice's results. In the atomistic results for the pure mode-II crack, the order is reversed in some cases.

The following are some of the likely reasons for the minor discrepancies between Rice's theory and the atomistic results.

(1) As in Schoeck's approach, the lattice resistance to dislocation motion, i.e., the Peierls stress, is not included. This will tend to make Rice's estimates of $K_{IIe}$ too low for high Peierls force crystals. As in Schoeck's case, we find that the deviation increases monotonically with the size of the Peierls barrier. Most striking is the mode-II result for $F^c$, where the narrowed dislocation and short range of force law combine to give a large deviation from Rice's curve.

(2) In Rice's calculation the dislocation center is precisely at the crack tip, and it is exactly half formed at the critical point of emission. For a pure mode-II nonequilibrium crack, we find that the dislocation just before emission is in fact right at the crack tip, and is half formed. This holds for all values of $l$ that we have used, as well as for the modified potentials. However, for the equilibrium crack, the position of the dislocation, and how completely formed it is, depend on the force law. For example, for an equilibrium crack in UBER, the separation between the crack tip and the dislocation center increases with decreasing $l$. For $l$=$l_{Cu}$, 0.7 $l_{Cu}$, and 0.55 $l_{Cu}$, the separations are about 1, 1.5, 2.5, respectively, in units of the lattice constant.

(3) The motion of the crack tip during emission is ignored.

(4) The interaction between mode-I and mode-II effects is ignored. As mentioned above, we find that mode-II loading creates some compressive stress in front of the crack tip, which can be countered by an applied mode-I stress. It is not clear how to evaluate such effects within Rice's model. However, one could imagine a procedure for evaluating the effects of $K_I$ on $\gamma_{us}$.

### E. Mode-I effects: lattice trapping

By lattice trapping, we mean the phenomenon that in all lattice models, the crack is stable at a particular lattice position for a range of loads (see Thomson[2]). This lattice trapping depends on the form of the force law. The general expectation is that the lattice trapping is smaller the longer is the range of the force. We have explored this question in our modeling with the result that with the UBER force law, the trapping is only about 5% for the "Cu" parameters, and even the observed trapping is probably due to the truncation of the force at the next-neighbor distance. For the extreme force, $F^c$, it is in the neighborhood of 35%. Thus the difference between the two conforms with the general expectation. We will find that in cases where the trapping is significant, the mixed mode behavior can become quite complicated.

### F. Mode-I–mode-II coupling

One of the entirely atomistic aspects of our results is the interaction between mode-I and mode-II loadings. In linear elastic theory, these act independently (see Lin and Thomson[10]). Dislocation emission from a crack tip along the cleavage plane is controlled exclusively by the mode-II loading, while cleavage is controlled exclusively by the mode-I loading. In addition, the shielding of the crack by an edge dislocation on the cleavage plane is pure mode-II shielding, with no shielding of the mode-I stress singularity. Finally, in linear elastic theory, a pure mode-II crack will never cleave, since there is no tensile force to open the crack; therefore dislocation emission is always favored. It is convenient to discuss mixed-mode loading with a "crack-stability" diagram (Lin and Thomson[10]). In linear elasticity, the cleavage curve in such a diagram [cf. Fig. 9(a)] is straight and normal to the $K_I$ axis and the emission curve is straight and parallel to the $K_I$ axis. In more elaborate calculations, the effects of mixed loading on the Griffith condition and dislocation emission depend in a complex way on the details of the atomic bonding in the crack tip region. Cheung, Yip, and Argon,[11] and earlier Argon,[12] have argued that shear softening by high tensile stress is a critical element in dislocation emission. Beltz and Rice[13] modeled such effects by broadening their framework to include coupled shear and tension. They concluded that in some cases, it is appropriate to include the effects of $K_I$ on $K_{IIe}$ by simply evaluating $\gamma_{us}$ under vanishing tensile stress (as opposed to fixed relative vertical positions of the blocks of atoms).

In our atomic calculations for the hexagonal lattice, a strong mode-I–mode-II interaction is found even using only our simple pair potential methodology. Figure 9(a) shows the results for the UBER force law, using the "Cu" parameters. Consider first the case of fixed mode-I load and increasing mode-II load. We see that $K_{IIe}$ is reduced by the mode-I load. We believe that this effect may be understood in a simple fashion in terms of the $\gamma_{us}$ parameter. As the mode-I load is increased, the two blocks whose relative displacement defines $\gamma_{us}$ are separated from each other, which as mentioned above reduces the corrugations in the potential as a function of parallel displacement. Thus $\gamma_{us}$, and in turn $K_{IIe}$, are reduced by the mode-I loading. Alternatively, one could think of the effect in terms of $\eta$. As discussed in Sec. III B, $\eta$ decreases under mode-I loading and $K_{IIe}$ is thus reduced according to Eq. (1.4). Both of these effects should be linear for small $K_I$, consistent with the behavior in Fig. 9(a). We also find a surprising crack-propagation effect

in the response of the crack to mode-II loading. As indicated in Fig. 4(a), with increasing mode-I loading, the crack extends (even well below the Griffith mode-I load) and at the same time builds up shear ahead of the crack until a dislocation is emitted from the crack tip. Then the crack tip retreats toward its original position, but only part way. As the mode-II load is increased, the process repeats itself. Thus, although mode-II loading by itself provides no driving force for crack opening, and the mode-I load is well below the Griffith value, the crack propagates. Such a process is an entirely atomic feature of dislocation emission, and corresponds to a curious mixed cleavage and emission event, which might be observable as a crack advance associated with emission.

Consider now the case of a nonequilibrium crack with less than the Griffith mode-I load, as the mode-II load is increased. We see in Fig. 9(a) that $K_{Ic}$ is reduced by the presence of the mode-II loading. This result may be due to the effect of the mode-II loading on the surface energy $\gamma_s$. To see this, consider the two-block geometry used to define $\gamma_{us}$. The surface energy is simply half the work required, per unit area, to pull the blocks apart in the direction perpendicular to the surface. But, if one first displaces the blocks in the parallel direction before separating them, as a mode-II load does, then the atoms at the interface between the blocks are imperfectly bonded, and less work is required to pull them apart. In fact, $\gamma_{us}$ measures precisely the imperfection of the bonding caused by lateral displacements. For small $K_{IIe}$, the symmetry of the lattice implies that the change in $\gamma_s$ is quadratic in $K_{IIe}$, consistent with the figure. If the blocks were displaced as far as the saddle point defining $\gamma_{us}$ before they were separated, then the new ($K_{II}$-dependent) surface energy would be $\gamma_s - \gamma_{us}/2$. (The factor of 1/2 comes from the conventions in defining $\gamma_s$ and $\gamma_{us}$; the former is defined per unit of total surface, so that pulling the blocks apart involves twice the surface energy, while the lateral displacement involves $\gamma_{us}$ with no extra factor of 2.) This presumably defines an upper bound for the effects of $K_{II}$ on $K_{Ic}$.

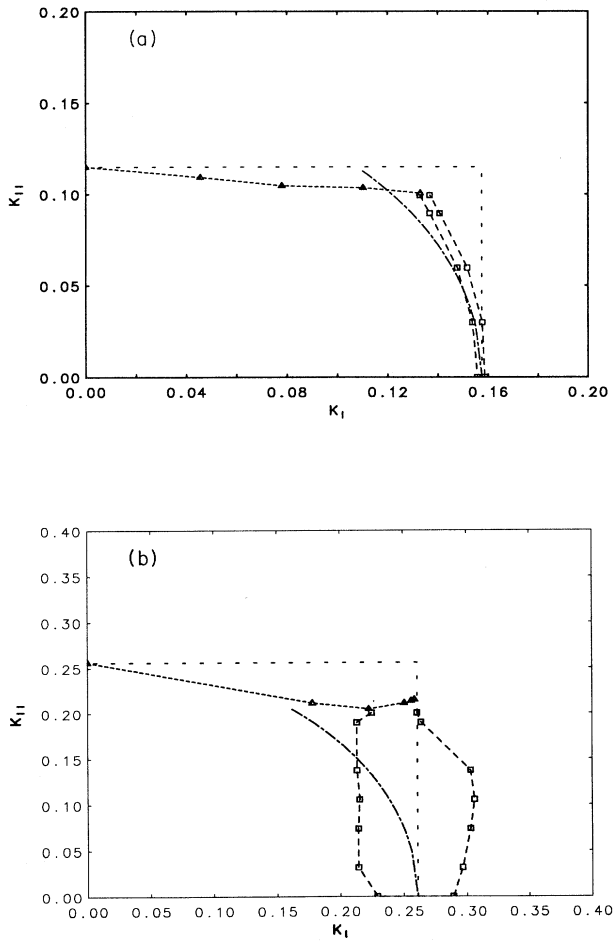


FIG. 9. Crack-stability diagram. Straight horizontal and vertical lines denote predictions of linear elasticity theory. Dot-dashed line indicates results of Sinclair-Finnis energy-release approach. Connected triangles indicate dislocation emission; connected squares indicate cleavage. For cleavage, crack-stability lines are given for both crack opening and closing; difference corresponds to lattice trapping. (a) $F^{\mathrm{UBER}}$ with $l = 0.55 l_{\mathrm{Cu}}$. (b) $F^{c}$ force law. Units for $K$ are $(k\sqrt{a})$.

For comparison, we include in Fig. 9(a) the prediction by the standard elastic analysis that a critical value of the elastic energy release, written in plane stress, $\mathcal{G}_C = (K_I^2 + K_{II}^2)/2\mu(1+\nu) = 2\gamma_s$, should represent the cleavage line (Sinclair and Finnis.[14]) This analysis assumes that the crack is always able to reach its absolute lowest-energy state and will not be trapped in a metastable, higher-energy state. Lin and Thomson[10] argue on heuristic grounds that the cleavage line is probably closer to being independent of $K_{II}$ and $K_{III}$, but no atomistic calculations have explored this question. We show that for our hexagonal lattice, the cleavage line follows neither of these criteria. In the UBER force law, the cleavage line is a relatively smooth curve lying between the vertical and circular cases. However, in the results for the $F^c$ laws, given in Fig. 9(a), it is very complex. Although we do not consider the latter results to be physically realistic, because of the short range of the force laws, the large difference between Figs. 9(a) and 9(b) indicates the large effect of the force law (at constant $\gamma_s$) on the crack-stability diagram. This suggests that the shape of the cleavage line appears to have little to do with the energy release function, $\mathcal{G}$, but is rather a complex mixture of crystallographic and force law effects.

This argument is not to deny that energy is released into the elastic field by the shear loading when the crack propagates under mixed mode-I–mode-II loading. Rather, the lattice bonding poses a necessary condition for existence of the equilibrium crack, and this (Griffith) condition has little to do with energy release. However, once the conditions for existence are satisfied, and the crack propagates under conditions where more elastic energy is expended than is necessary to make the surface, then this excess energy is available to drive the crack to high velocity. Hence, a crack under mixed mode loading with the mixed load stability shown in Fig. 9(a), is more unstable than when loaded in pure mode I.

## IV. CONCLUSIONS

The salient features of the results described above are the following. The dislocation emission criterion is described accurately by a parameter related to dislocation structure, namely the maximum strain $\eta$ of an incipient crack-tip dislocation. This parameter gives $K_{\mathrm{IIe}}$, for a broad range of model force laws, to an accuracy of about 5%. Evaluation of two continuum-based theories due to Rice and Schoeck shows that both of these theories agree surprisingly well with the atomistic results. However, the atomistic results show that some of the assumptions underlying both of these theories are quite flawed; in particular, the maximum strain $\eta$ of the dislocation core depends on its position relative to the crack, the critical configuration is not necessarily right at the crack tip, and the crack tip moves during emission. Finally, we have shown that in atomistic calculations, mode-I–mode-II interactions are obtained which can be understood via the effects of stress on the unstable stacking energy, the dislocation width, and the surface energy.

## ACKNOWLEDGMENTS

We would like to first acknowledge discussions with J. Rice regarding his unstable stacking fault analysis and plane stress elasticity, which we found very helpful in analyzing the comparison between our results and his. It is also a pleasure to acknowledge helpful discussions with I.H Lin, and we are very grateful to Dr. John Simmons of NIST for making available to one of us (S.J.Z.) an SGI workstation computer on which much of the numerical and graphical computations were done. The work at Washington University was supported by the Department of Energy under Grant No. DE-FG02-84ER45130, and a portion of the work at NIST was supported by ONR.

[1] J. R. Rice and R. Thomson, Philos. Mag. **29**, 73 (1974).
[2] R. Thomson, Solid State Phys. **39**, 1 (1986).
[3] J. Weertman, Philos. Mag. **43**, 1103 (1981).
[4] G. Schoeck, Philos. Mag. **63**, 111 (1991).
[5] J. R. Rice, J. Mech. Phys. Solids **40**, 239 (1992).
[6] J. P. Hirth and J. Lothe, *The Theory of Dislocations* (Wiley, New York, 1982).
[7] R. Thomson, S. J. Zhou, A. E. Carlsson, and V. K. Tewary, Phys. Rev. B **46**, 10 613 (1992).
[8] J. H. Rose, J. R. Smith, and J. Ferrante, Phys. Rev. **28**, 1835 (1983).
[9] F. C. Frank and J. W. Steeds, in *The Physics of Metals: 2. Defects*, edited by P. B. Hirsch (Cambridge University Press, New York, 1975).
[10] I.-H. Lin and R. Thomson, Acta Metall. **34**, 187 (1986).
[11] K. Cheung, S. Yip, and A.S. Argon, J. Appl. Phys. **69**, 2088 (1991).
[12] A. S. Argon, Acta Metall. **35**, 185 (1987).
[13] G. E. Beltz and J. R. Rice, Acta Metall. **40**, 5321 (1992).
[14] J. E. Sinclair and M. W. Finnis, in *Atomistics of Fracture*, edited by R. Latanision and J. Pickens (Plenum, New York, 1983), p. 1047.
[15] A. J. Foreman, M. A. Jaswon, and J. K. Wood, Proc. Phys. Soc. **64A**, 156 (1951).